A numerical study on the wave loading on offshore structures of different cross-sectional geometries under the action of regular waves

Guilherme Fuhrmeister Vargas
ORCID: https://orcid.org/0000-0002-6923-6842
Federal University of Rio Grande do Sul (UFRGS) – Institute of Hydraulic Research (IPH), Brazil
E-mail: guilhermef.engenharia@gmail.com
Bruno Alvarez Scapin
ORCID: https://orcid.org/0000-0001-8013-468X
Federal University of Rio Grande do Sul (UFRGS) – Institute of Hydraulic Research (IPH), Brazil
E-mail: bruno.scapin@hotmail.com

Abstract
Coastal engineering and maritime hydraulics have experienced significant development over the years with the construction of bridges, oil exploration platforms, and ports, highlighting the importance of studying and quantifying the efforts resulting from wave loads on these structures. The present work aims to identify how a variation in the geometry of the cross-section, along the wave climate, can modify the magnitude of the wave loadings experienced by the structure. The open-source computational code OpenFOAM v. 4.1 was applied in the considered cases, along with the OlaFlow extension, considering the application of a structured mesh, the VOF (Volume of Fluid) methodology for representing the free surface, and the turbulence modeling according to Reynolds averaged equations (RANS). The results demonstrated that the shape of the cross-section plays an important role in the efforts experienced by the structure, and this influence is directly related to a characteristic length, whose intensification causes an increase in the magnitude of the experienced horizontal force. Likewise, by defining important dimensionless parameters, it was possible to obtain approximate expressions to determine the maximum wave force on the structures. The results and analyses carried out demonstrated that the force value calculated according to this approximation methodology is quite adequate, presenting relative errors smaller than 11,00%, corresponding to a relevant simplified approach for the determination of the maximum wave loads experienced by the structures, which can be important for proper design and analysis.
Keywords: Wave Loading. Offshore Structures. Computational Fluid Dynamics. OpenFOAM. OlaFlow. RANS.

1. Introduction

Over the last few years, there has been a considerable development in coastal engineering construction techniques. This fact can be associated with the great interest in exploring ocean resources, such as oil and renewable energy sources (where wave, tidal and wind energy stands out), which has led to the execution of several onshore and offshore structures (Kumar; Savitha; Al Mamun, 2018). On the other hand, Faltinsen (2015) emphasizes that the waves hydrodynamics involves many complex fluid mechanics phenomena, such as the influence of inertial forces and viscous forces, vortex induced vibrations, vortex induced motions, structural resonance, and slamming. According to the author, all these aspects must be carefully analyzed and considered in

coastal engineering projects, as extreme wave conditions can damage the structures, resulting in important economic losses and casualties (Qiu *et al*., 2022).

In this context, computational numerical modeling emerges as an important tool for the study and design of coastal structures, complementing experimental studies and making it possible to understand the complex phenomena associated with wave hydrodynamics (Mohapatra; Soares, 2019; Li *et al*., 2022). With the advancement of computational techniques, Computational Fluid Dynamics (CFD) models allow the analysis of several important structural aspects regarding the wave loads on coastal structures (Chen *et al*., 2022). Among these, the Reynolds Averaged Navier-Stokes (RANS) method for turbulence modeling stands out for its robustness, which, combined with its computational cost-effectiveness, makes it possible to simulate cases of considerable complexity in a relatively short period of time (Elhanafi *et al*., 2017).

However, the recent work published by Dutta, Bihs, and Afzal (2022) points out that the main tools available in the literature for calculating forces on coastal structures refer to cylinders of circular cross-section, demonstrating that further studies regarding different section geometries are required. This fact becomes even more evident when one observes the need to develop practical methodologies for estimating wave loads, which corresponds to an important contribution to the engineering of coastal structures (Bredmose *et al*., 2016).

In order to fill these gaps, the main objective of this work is to numerically analyze the influence of wave forces on offshore vertical structures composed of different cross-section geometries. Therefore, the present study aims to contribute to the development and execution of structures that are under the action of wave loading as well as to emphasize the importance of geometry in the attenuation of unfavorable effects.

2. Numerical methodology

The free and open-source computational code OpenFOAM v. 4.1 was applied to carry out the simulations, together with the OlaFlow extension (Higuera, 2016), which implements the hydrodynamics of regular waves in the main code. The mathematical modeling of the problem, according to the RANS methodology, consists of solving the Navier-Stokes and the continuity equations in average terms, which are given, respectively, in tensor notation, by the following expressions:

$$\frac{\partial \overline{u}_i}{\partial t} + \overline{u}_j \frac{\partial \overline{u}_i}{\partial x_j} = -\frac{1}{\rho}\frac{\partial \overline{P}}{\partial x_i} + \frac{\partial}{\partial x_j}\left(v\frac{\partial \overline{u}_i}{\partial x_j} - \overline{u_i'u_j'}\right) + g_i \tag{1}$$

$$\frac{\partial \overline{u}_j}{\partial x_j} = 0 \tag{2}$$

where u_i represents the velocity, P the pressure, x_i the position, g_i the gravitational acceleration, ρ the density and v the kinematic viscosity of the fluid. The bar over some variables of the previous equations indicates that they consider average aspects (due to the Reynolds decomposition).

The term $\overline{u_i'u_j'}$ is known as the Reynolds stress tensor and represents additional unknown variables to the system of equations, requiring its correct representation. To solve this additional term, it is necessary to apply the Boussinesq hypothesis, which is based on an analogy between the turbulent stresses and the viscous stresses of laminar flow, suggesting that the stresses associated with turbulence are proportional to the mean flow velocity gradient. These considerations lead to a coefficient of proportionality known as turbulent viscosity (Kajishima; Taira, 2016). Therefore, the Navier-Stokes equation can be rewritten as:

$$\frac{\partial \overline{u}_i}{\partial t} + \overline{u}_j \frac{\partial \overline{u}_i}{\partial \overline{x}_j} = \frac{\partial Pm}{\partial x_i} + \frac{\partial}{\partial x_j}\left([v_t + v]\left[\frac{\partial \overline{u}_i}{\partial x_j} + \frac{\partial \overline{u}_j}{\partial x_i}\right]\right) + g_i \tag{3}$$

where Pm represents the modified Boussinesq pressure and ν_t the turbulent viscosity. To represent this last variable, turbulence models are generally applied, with the $\kappa - \varepsilon$, $\kappa - \omega$ and $\kappa - \omega$ SST models being the most known and widespread. The latter combines the precise formulation of the κ-ω model in the regions close to the walls with the robustness of the κ-ε model for the free current representation (Könözsy, 2019). For these reasons, the κ-ω SST model proves to be quite suitable for the analyzes of the present work.

2.1 Numerical formulation of the OpenFOAM code

OpenFOAM relies on the numerical methodology of finite volumes, which consists of dividing the domain into several discrete control volumes where the variables and constants of the equations are referenced in their centroids, which are later integrated throughout the domain. The values of the variables on the element faces are determined through interpolations from the values calculated on the volume centroids (Jasak, 2009).

The OlaFlow extension allows the resolution of biphasic problems with wave generation and consists of a modification in the existing interFoam solver, which is based on the methodology known as Volume of Fluid (VOF) and applies a variable named volume fraction that presents variations between 0 (filled only by air) and 1 (completely filled by water), indicating the air-water interface. For the correct identification of this interface, it is necessary to apply an artificial compression, originating a term that is added to the transport equation and is only active in the surface region. This solution is obtained by the MULES calculation method (Multidimensional Universal Limiter for Explicit Solution). The velocities and pressure are obtained by the PIMPLE algorithm, which is based on the PISO algorithm (Pressure Implicit with Splitting of Operators) and on the SIMPLE algorithm (Semi-Implicit Method for Pressure-Linked Equations), ensuring a good approximation and convergence of the results (Higuera, 2016). The wave hydrodynamics theories implemented by OlaFlow are: first, second and fifth order Stokes, Cnoidal, Stream function and Solitary waves. All of these introduce a non-uniform velocity profile to the domain inlet boundary and the wave motion is generated by a piston wavemaker (Lee *et al*., 2021).

2.2 Numerical domain

The calculation domain (Figure 1) was designed in the shape of a wave tank, divided into the following boundaries: inlet, outlet, top, bottom, side 1 and side 2. The structure analyzed in all cases is positioned in such a way that the center of its lower base coincides with the central vertical line of the domain, being sufficiently distant from the inlet and outlet, in order to avoid any perturbation from these boundaries. Likewise, it is assumed that the structure has a height equal to the vertical dimension of the domain (L_z). The dimensions L_x, L_y and L_z depend on the case of analysis, so their values will be detailed later in this work.

2.3 Initial and boundary conditions

The conditions of regular wave generation, sponge layer, outflow, and free slip are applied, respectively, to the inlet, outlet, top, and to both sides. On the other hand, the non-slip condition is applied to the bottom of the domain and the vertical structure. Table 1 shows the conditions considered on the boundaries of the domain, according to their nomenclatures in the OpenFOAM code.
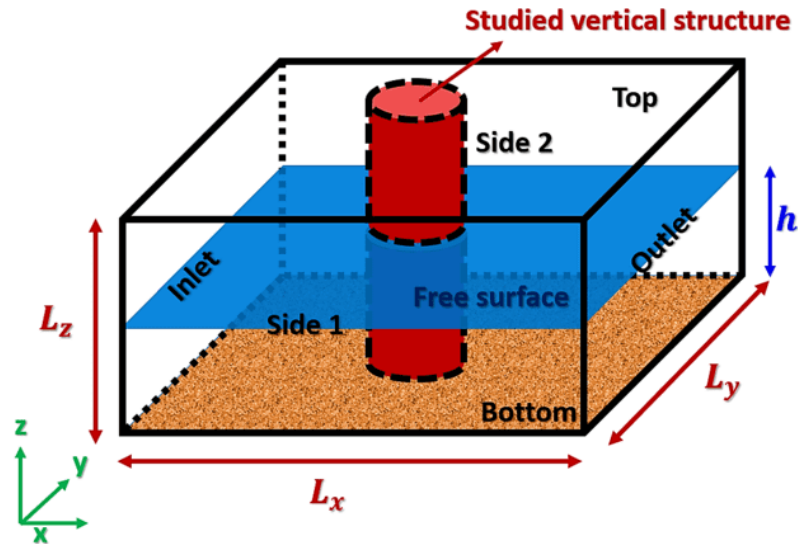
Figure 1 - Characteristics of the numerical domain.

Table 1 – Boundary conditions applied to the simulations.

Boundary	Velocity condition	Pressure condition
Inlet	*waveVelocity*	*fixedFluxPressure*
Outlet	*waveAbsorption3DVelocity*	*fixedFluxPressure*
Top	*pressureInletOutletVelocity*	*totalPressure*
Bottom	*noSlip*	*fixedFluxPressure*
Side 1	*slip*	*fixedFluxPressure*
Side 2	*slip*	*fixedFluxPressure*
Structure	*noSlip*	*fixedFluxPressure*

The null internal field condition was applied for the pressure and velocity, while 0,50 s was the adopted initial time step. However, this time step is allowed to be modified as the simulations advance, always maintaining the Courant number below 0,80, ensuring numerical stability and convergence to obtain sufficiently accurate results.

2.4 Characteristics of the numerical mesh

A structured-type mesh was applied to the simulations, dividing the domain into small hexahedral elements. It was generated using the blockMesh tool, which is part of the OpenFOAM code, and represents a full-scale domain in the analyzed cases.

Figure 2 shows a schematic of the numerical mesh applied in this work, where one can observe the configurations of the elements for the rectangular structures (Figure 2a) and for the cylindrical structures (Figure 2b). This last configuration forces the elements to be radially distributed in the regions close to the structure, resulting in a domain slightly wider than the one observed in the rectangular structures. For calculation and convergence purposes, a uniform discretization (Δx, Δy and Δz) of 0,50 m was adopted for the numerical mesh elements.
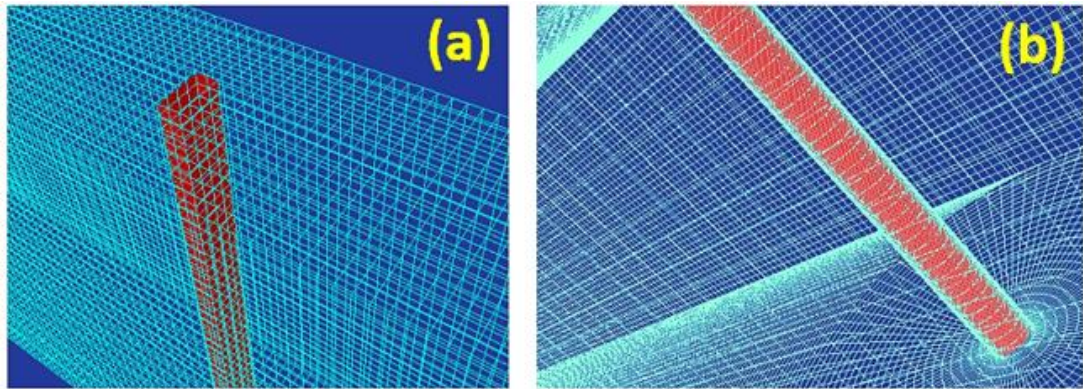
Figure 2 - Detail of the numerical mesh applied in the analyses, considering rectangular (a) and cylindrical (b) structures.

2.5 Analysis cases considered in this work

The studied cases were divided into 3 main scenarios. The first concerns the validation of the numerical code, which was performed by comparing the results generated by the considered mathematical model with those obtained in the experiment described in the work by Mo *et al.* (2007). This study was carried out in the large wave tank at the Coastal Research Center in Hanover (Germany), and its characteristics are presented below:

- L_x =309,00 m, L_y = 5,00 m, L_z = 7,00 m;
- Water level (h): 4,76 m;
- Diameter of the cylindrical structure (D): 0,70 m;
- Wave height (H): 1,20 m;
- Wave period (T): 4,00 s.

The second scenario aims to investigate four different types of cross sections (Figure 3) under the action of a regular wave of 2,50 m height and 6,00 s period. Such geometries represent the usual cases applied to coastal structures.
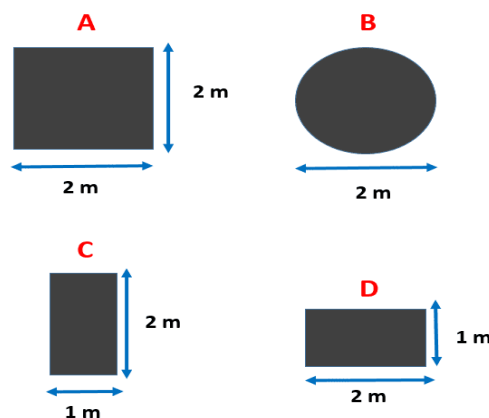

Figure 3 - Analyzed cross-sectional geometries.

In the third and last scenario, a rectangular section 1,00 m long and 2,00 m wide is adopted (type C section), arranged transversely to the flow (geometry generally associated with a considerable flow separation), which is subject to the action of the combination of wave heights and wave periods arranged in Table 2.

Table 2 – Cases and wave characteristics applied in the numerical simulations of the third scenario.

Case	H (m)	T (s)	Applied wave theory
H1	1,50	6,00	Stokes II
H2T1	2,50	6,00	Stokes V
H3	3,50	6,00	Stokes V
T2	2,50	10,00	Stokes V
T3	2,50	13,00	Stokes V

In the second and third scenarios, the depth (h) and the adopted dimensions of L_x and L_z were 15 m, 150 m, and 20 m, respectively. For the case corresponding to the cylindrical structure, the adopted value of L_y was 30 m due to the distribution of the radial mesh elements in this case. In other cases, 10 m was considered for L_y.

3. Results

All scenarios and their respective considerations will be presented separately in this section, promoting a more concise and detailed analysis of each case.

3.1 Validation of the numerical method

In order to verify whether the numerical grid discretization and the applied boundary conditions adequately represent a real case, the experimental study carried out by Mo *et al.* (2007) was compared with the present numerical model. To quantify the differences between the results, the coefficient of determination (R^2) and the Normalized Root Mean Square Error ($NRMSE$) were applied, which are described, respectively, by the following expressions:

$$R^2 = \frac{\left(\sum X_e . X_m - \sum X_e . \sum \frac{X_m}{N}\right)^2}{\left(\sum X_e{}^2 - \frac{(\sum X_e)^2}{N}\right)\left(\sum X_m{}^2 - \frac{(\sum X_m)^2}{N}\right)} \tag{4}$$

$$NRMSE = \frac{100}{Max_{X_e} - Min_{X_e}} \sqrt{\frac{1}{N}\sum(X_e - X_m)^2} \tag{5}$$

where N, X_e, X_m, Max_{X_e}, and Min_{X_e} represent, respectively, the total number of data analyzed, the experimental values, the associated values of the numerical model (at the same time), and the maximum and minimum values of the experimental study. The closer the R^2 value is to 1 and the smaller the $NRMSE$, the better the numerical model will be at representing the physics involved in the analysis.

Figure 4 shows the comparison between the time histories of the horizontal forces (F_x) on a vertical cylinder (their values have been dimensionalized for better visualization). Through these series, it is observed that the numerical model reproduces the horizontal forces on the structure quite satisfactorily, considering the adopted discretization and the mesh configuration, which can be correlated to the obtained R^2 and $NRMSE$ values. Therefore, it is considered that the numerical model is adequate to satisfy the objectives of the present work and should therefore be applied in all subsequent cases of analysis.
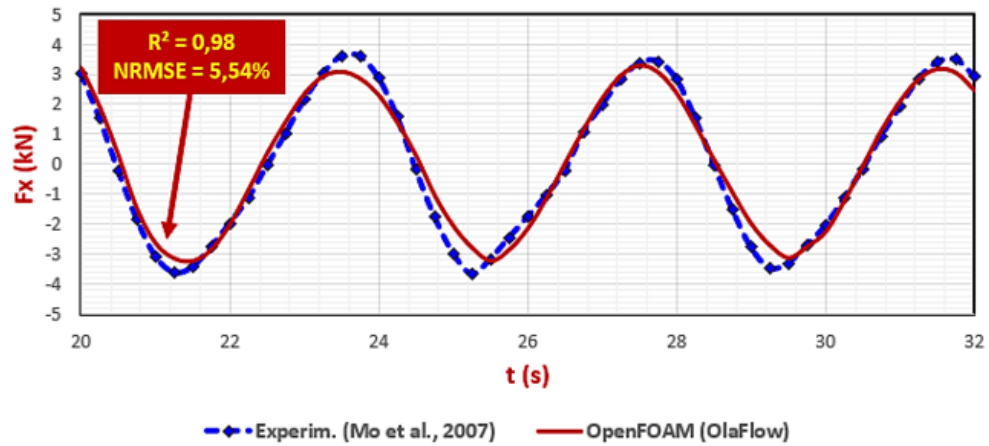
Figure 4 – Comparisons of the observed results for the horizontal load on a vertical cylinder, considering the adopted numerical model and the experimental study carried out by Mo *et al*. (2007).

3.2 Influence of the cross-section geometry

The four proposed cross-section geometries were analyzed considering the action of the same regular wave. A comparison between the velocity fields is shown in Figure 5, for the same instant of time, which marks the passage of a wave crest through the structure.
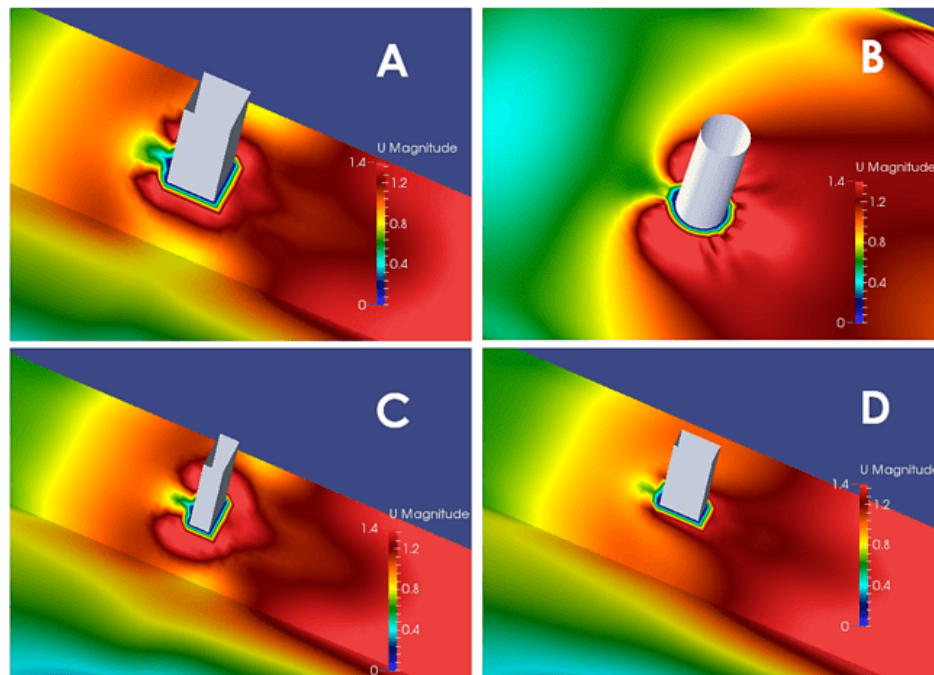

Figure 5 - Comparison between the velocity fields considering the analyzed cross-section geometries during the passage of a wave crest.

In the previous figure, it can be observed that the geometries A and C are those that cause an increase in the magnitude of the velocity in the posterior region of the structure. On the other hand, section B (circular) shows a better distribution of velocities around the structure, favoring the flow hydrodynamics. Section D is the one that presents the smallest magnitudes of velocities in the vicinity of the structure, due to its frontal area, which is smaller than that of the other geometries. Such behaviors lead to the conclusion that sections with the same frontal section should have their

longitudinal lengths increased in order to reduce the wake of vortices posterior to the structure, in the same way as to decrease the magnitude of velocity in the regions around the rigid body.

In figure 6, one can observe the time histories of the horizontal loads for the different geometries considered in the study, together with the RMS values of this variable. Thus, it can be observed that the type A section is the one that presents the greatest horizontal forces, while the D section presents the smallest loads. Similarly, section C is the one that presents the highest loading values after section A, followed by the type B section.
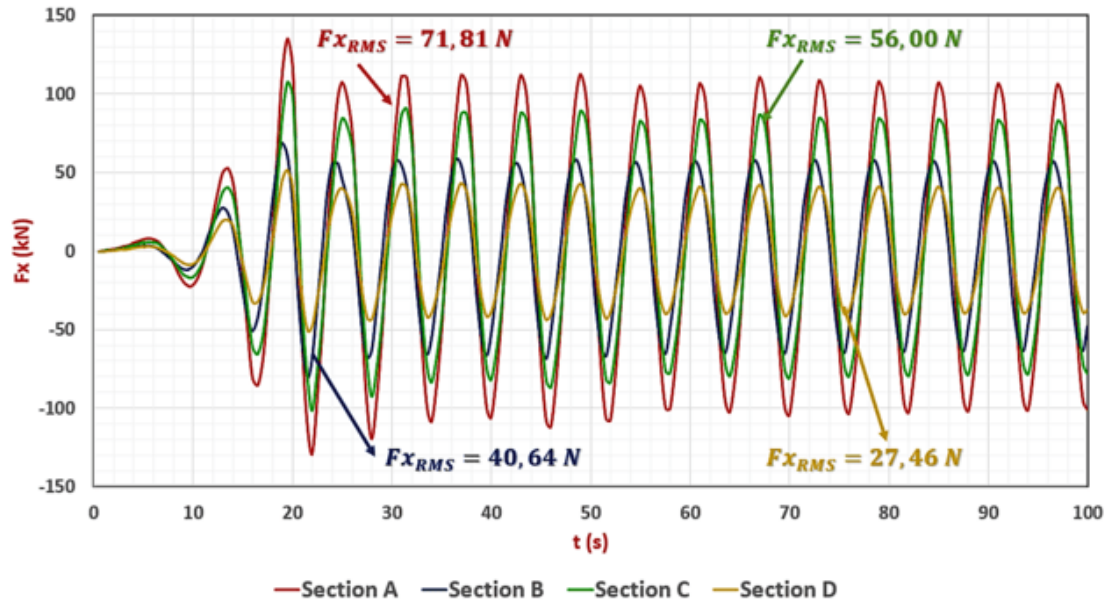

Figure 6 - Time histories of the horizontal loading for the different cross-section geometries considered.

All these results can be correlated with the velocity magnitudes observed in Figure 5, leading to the conclusion that the sections of smaller frontal areas with rounded edges are correlated with smaller horizontal wave loads. This behavior is very close to that observed in the hydrodynamics of currents, demonstrating that a change in the geometry of the cross-section of the structure can reduce the horizontal load by up to 62%, considering a comparison of the RMS values of F_x in the A and D cases.

3.3 Influence of wave height and wave period on a structure of defined cross section

Considering the increase in velocity magnitude and the characteristic of the wake zone formed in the posterior region of the structure, together with the fact that it is a geometry widely applied in coastal structures, the type C section was adopted as a case of analysis. Therefore, the influence of the wave height and wave period on the horizontal wave loading was studied according to the cases shown in Table 2, whose time histories are presented on Figures 7 and 8.

According to the graphs presented in Figure 7, the horizontal force shows a considerable intensification with the increase in wave height. On the other hand, the horizontal loading variation as a function of the wave period is much less significant (Figure 8), with its maximum and minimum values being quite similar for the three analyzed periods. However, as one can observe in the analyzed cases, there is an increase in the horizontal force with the decrease of the wave period. This fact, combined with the intensifications caused by the increase in wave height, could damage the structures due to the higher loads experienced.
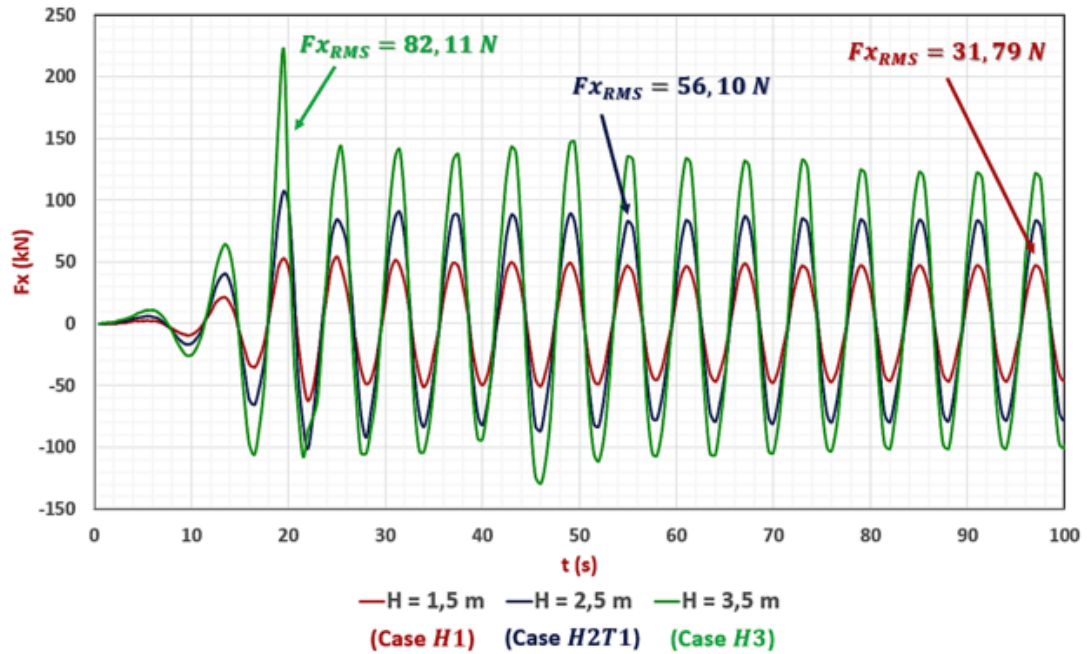
Figure 7 - Time histories of the horizontal loading on a C-type cross-sectional structure, considering three wave heights.
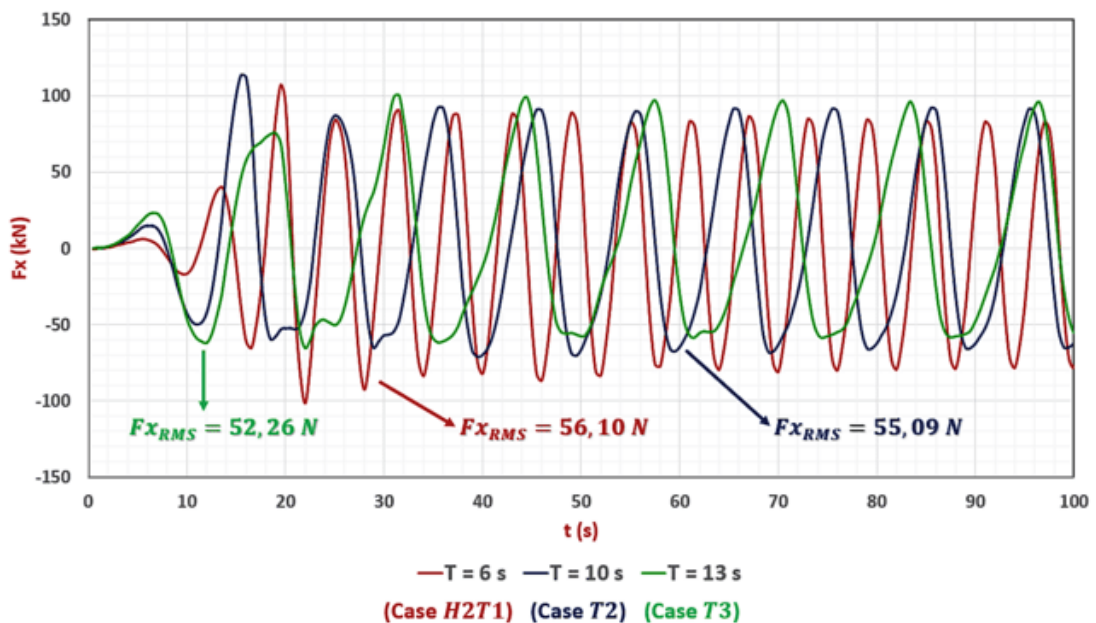

Figure 8 - Time histories of the horizontal loading on a C-type cross-sectional structure, considering three wave periods.

Considering the same effects caused by variations in wave height and wave period, we propose to apply dimensional analysis concepts to the cases analyzed in this section. Such a strategy is suitable since it allows one to model the associated hydrodynamics more concisely and generically, making it possible to extend the results of these cases to other cross-section geometries.

The first parameter to be considered in the dimensional analysis is the characteristic length (L_c) of the structure. It is defined based on the cross-sectional area "A_s" (which provides an idea of the distribution of the structure in the plane), the wetted perimeter "P_w" (associated with the contact of the water with the walls), the dimension along the wave propagation direction "B" (this length represents how large the dimension of the structure is compared to the incident wavelength) and the

9

diagonal of the cross section "d_s" (which quantifies the aspect ratio of the rigid body). The following expression defines the characteristic length of the structure:

$$L_c = \frac{A_S \cdot P_W}{d_S \cdot B}$$ (6)

After applying the pi theorem (Curtis, 1982) and some combinations between the dimensionless groups, a characteristic length of the structure (X_a) relative to the wave climate can be defined. Similarly, it is possible to present a dimensionless force (F_{x_a}) relative to the characteristic of the incident wave. The following expressions present the respective variables:

$$X_a = \frac{H.T}{\sqrt{\frac{L_c^3}{g}}}$$ (7)

$$F_{x_a} = \frac{F_x}{\frac{\rho.h.\sqrt{g.L_c^5}}{T}}$$ (8)

Based on these dimensionless parameters, the maximum, minimum, and RMS values of all the time histories of the observed horizontal forces were calculated (relative to the cases presented in Table 2). Afterwards, these forces were adimensionalized according to expression 8, resulting, respectively, in the values of F_1, F_2 and F_3. The scattering of these parameters is presented in the graphs of Figure 9, where a linear fit is suitable for all of them. In this same figure, it is possible to observe that the dimensionless wave force tends to increase proportionally to the relative characteristic length.
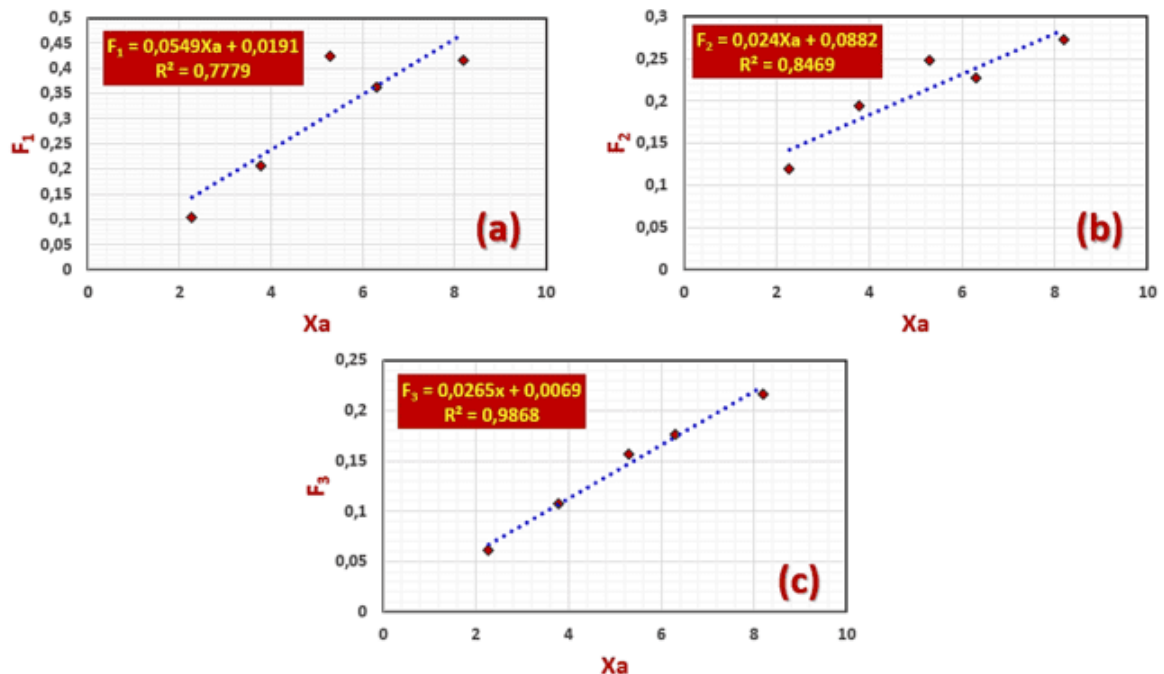

Figure 9 - Scattering of maximum (a), minimum (b) and RMS (c) values of the horizontal loads, in dimensionless terms.

The functions obtained for the dispersions presented in Figure 9 allow us to bring the values of F_1, F_2 and F_3 to a dimensional form, through the application of expression 8. This leads to the approximate determination of the maximum ($F_{x_{Max}}$), minimum ($F_{x_{Min}}$) and RMS ($F_{x_{RMS}}$) values of the horizontal force for the different geometries of Section 3.2 and for the experimental case

described in the work by Mo *et al*. (2007). These values, together with the absolute values of the maximum horizontal force ($F_{x_{Abs}}$) and the characteristics of each case, are shown in Table 3.

Table 3 – Characteristics of the cases considered for verification of the proposed method to estimate the maximum, minimum and RMS values of the wave loads.

Case	H (m)	T (s)	h (m)	L_c (m)	X_a	$F_{x_{Abs}}$ (kN)	$F_{x_{Max}}$ (kN)	$F_{x_{Min}}$ (kN)	$F_{x_{RMS}}$ (kN)
A	2,50	6,00	15,00	5,66	3,49	**134,95**	125,63	102,51	59,26
B	2,50	6,00	15,00	4,93	4,29	**80,43**	107,76	80,93	51,03
C	2,50	6,00	15,00	5,37	3,78	**107,47**	118,36	93,46	55,92
D	2,50	6,00	15,00	2,68	10,69	**51,17**	55,96	31,84	26,80
Mo *et al*. (2007)	1,20	4,00	4,76	1,73	6,62	**3,65**	5,59	3,61	2,67

In the previous table, it is possible to observe that in some cases the value of $F_{x_{Max}}$ is closer to $F_{x_{Abs}}$, while in other cases this value is better approximated by $F_{x_{Min}}$. This demonstrates that it is necessary to establish some criterion to determine which value will represent a better approximation for the highest magnitude of the horizontal force observed in each case.

In order to formulate a criterion to determine the best approximation function for the magnitude of the maximum observed wave load, the relative differences between the values of $F_{x_{Abs}}$ and $F_{x_{Max}}$ are analyzed, in the same way as $F_{x_{Abs}}$ and $F_{x_{Min}}$. These relative differences are demonstrated in the graph of Figure 10, from where it is possible to identify the intervals (in terms of X_a) where each function is closest to zero (indicating a better approximation). The respective observed intervals and the best approximation function for each case are summarized in Table 4.
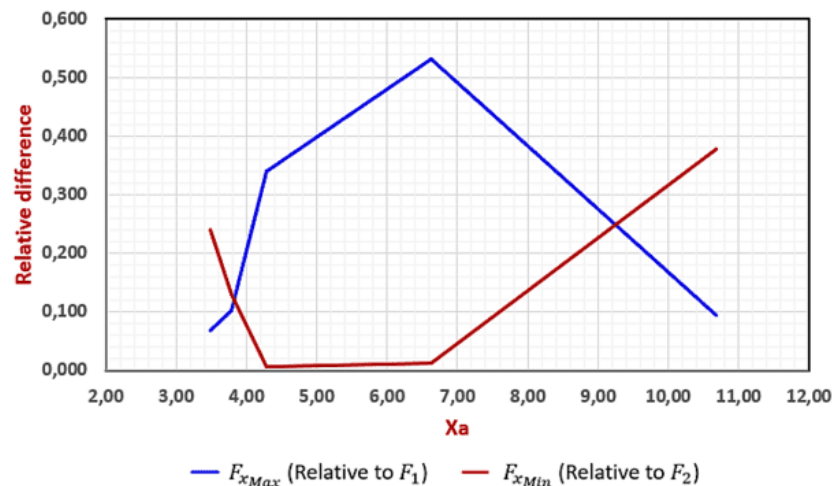

Figure 10 - Relative differences observed for $F_{x_{Max}}$ and $F_{x_{Min}}$, when compared to $F_{x_{Abs}}$ values.

Table 4 – The most suitable function for estimating the value of $F_{x_{Abs}}$, according to the range of the variable X_a.

Interval	Best estimated by
$X_a < 3,80$	F_1
$3,80 < X_a < 9,20$	F_2
$X_a > 9,20$	F_1

After defining the criteria according to the X_a interval, it is possible to estimate the magnitude of the maximum wave load ($F_{x_{Me}}$) on the structure. The estimated values, together with the $F_{x_{Abs}}$ values, referring to the cases highlighted in Table 3, are presented in Table 5.

Table 5 – Approximate wave loading values according to the analysis cases, together with the relative errors and the relationship with the estimated RMS value of the experienced horizontal force.

Case	L_c (m)	X_a	$F_{x_{Abs}}$ (kN)	$F_{x_{Me}}$ (kN)	ε (%)	$\dfrac{F_{x_{Me}}}{F_{x_{RMS}}}$
A	5,66	3,49	134,95	125,63	6,90	2,12
B	4,93	4,29	80,43	80,93	0,63	1,59
C	5,37	3,78	107,47	118,36	10,13	2,12
D	2,68	10,69	51,17	55,96	9,34	2,09
Mo *et al.* (2007)	1,73	6,62	3,65	3,61	1,17	1,35
				Average	5,64	1,85

Considering the previous table, it is observed that in the range considered ($3,50 < X_a < 11,00$), the present proposed methodology provides values very close to those observed in each case, presenting an average relative error close to 6,00%, while the maximum relative error is less than 11,00%. Furthermore, it is noticed that the value of $F_{x_{RMS}}$ is approximately equal to half of the value of $F_{x_{Me}}$.

In the graph of Figure 11, one can observe that $F_{x_{Abs}}$ grows with the increase of L_c, demonstrating that this characteristic length is fundamental to determining the maximum wave loads experienced by the structure. In this figure, it is also observed that the proposed methodology satisfactorily approximates the absolute values of the maximum loads, suggesting that the $F_{x_{Abs}}$ variation rate increases for L_c values smaller than 2,70 m and for values greater than 5,00 m.
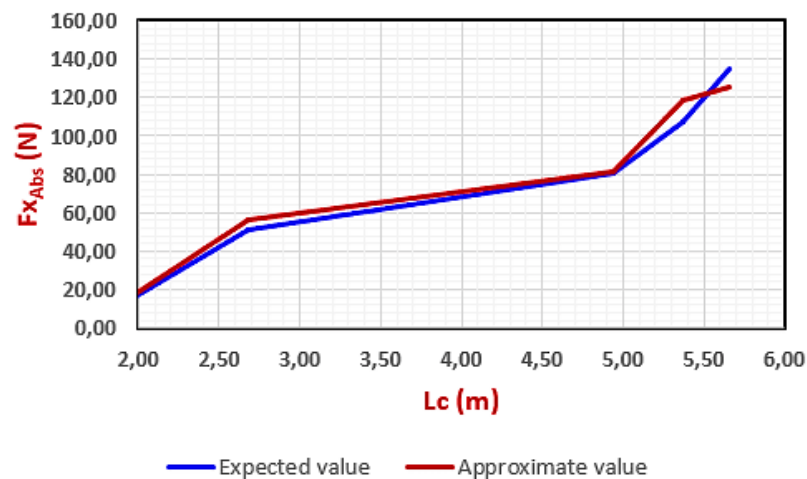

Figure 11 - Variation of $F_{x_{Abs}}$ with the increase of characteristic length (L_c).

Seeking to evaluate the influence of the relative characteristic length X_a on wave loadings, the $F_{x_{Abs}}$ values (considering both observed and approximate values) were dimensionless by applying expression 8. The graph shown in Figure 12 demonstrates once again that the values estimated by the present methodology are quite adequate since the curves show good agreement. In addition, one can observe that the value of F_{x_a} tends to increase with the increase of X_a. However, the curve also shows that the dimensionless force tends to increase for X_a values lower than 4,00, which strongly

suggests that the F_{x_a} values can oscillate with the variation of the relative characteristic length. This fact is probably associated with the different hydrodynamic conditions resulting from the combination of wave height and wave period, where inertia and drag play important roles on wave loading.
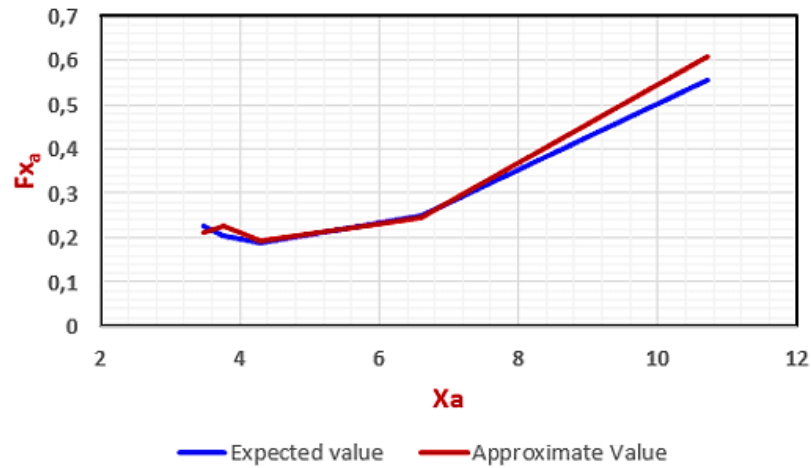

Figure 12 - Variation of F_{x_a} with the increase of relative characteristic length (X_a).

4. Conclusions

The present work applied the OpenFOAM open-source computational code, together with the OlaFlow extension, the RANS modeling methodology, and the VOF method to represent the free surface. The simulations were planned in order to verify how a modification in the cross-section geometry of an offshore structure influences the magnitude of the experienced wave loading.

The results demonstrated that the geometry of the cross-section can be represented in terms of a dimensionless length L_c, which takes into account the main geometric aspects that modify the associated hydrodynamics. Thus, higher values of L_c result in higher magnitudes of the wave loading.

On the other hand, assuming that the hydrodynamics associated with the geometry of the cross section is similar for the same wave characteristics, it was proposed to represent the problem according to the principles of dimensional analysis. In this context, the relative characteristic length (X_a) and the dimensionless wave load (F_{x_a}) were proposed to correlate the wave climate to the geometry of the cross section and the maximum experienced horizontal force. Through the results, it was found that F_{x_a} intensifies with the increase of X_a, also suggesting that the dimensionless force increases for X_a values lower than 4,00. However, for a more detailed study it would be necessary to extend the analysis to X_a values lower than 4,00, as well as to values greater than 11,00.

In addition, the X_a and F_{x_a} parameters allowed the adjustment of three approximate linear functions, which estimate the magnitude of the maximum, minimum, and RMS values of the horizontal force experienced by the structure. Depending on the value of X_a, the magnitude of the maximum observed loading will be better adjusted by the maximum or minimum values calculated by the approximation functions. A criterion based on intervals of X_a was proposed, allowing these expressions to provide very approximate estimates for the maximum observed horizontal force magnitude. The maximum observed relative error, according to this approximation methodology, was less than 11,00%, indicating good adherence and accuracy of this model for the considered X_a interval.

In general, the results obtained in this work demonstrated that the characteristic length L_c is quite influential in the observed maximum load. Likewise, the methodology for estimating the magnitude of the observed maximum horizontal force proved to be quite adequate in the range

considered in the analyses. This result is very motivating since it corresponds to a practical estimate of the associated wave loading, depending on the wave climate and rigid body geometry, favoring the correct design and development of offshore structures. In addition, the present work makes evident the important influence of the proposed dimensionless parameters, showing that a more detailed study is necessary for values outside the considered application range, which may make the proposed methodology even more robust.

Acknowledgements

References

Bredmose, H., Dixen, M., Ghadirian, A., Larsen, T. J., Schløer, S., Andersen, S. J., ... & Hanson, T. D. (2016). DeRisk—accurate prediction of ULS wave loads. Outlook and first results. *Energy Procedia*, 94, 379-387.
https://doi.org/10.1016/j.egypro.2016.09.197

Chen, L., Zhou, J., Duan, J., Wang, X., & Xie, Y. (2022). Wave loads on high-rise pile cap structures and mitigation approach. Ocean Engineering, 243, 110189.
https://doi.org/10.1016/j.oceaneng.2021.110189

Curtis, W. D., Logan, J. D., & Parker, W. A. (1982). Dimensional analysis and the pi theorem. *Linear Algebra and its Applications*, 47, 117-126.
https://doi.org/10.1016/0024-3795(82)90229-4

Dutta, D., Bihs, H., & Afzal, M. S. (2022). Computational Fluid Dynamics modelling of hydrodynamic characteristics of oscillatory flow past a square cylinder using the level set method. *Ocean Engineering*, 253, 111211.
https://doi.org/10.1016/j.oceaneng.2022.111211

Elhanafi, A., Fleming, A., Leong, Z., & Macfarlane, G. (2017). Effect of RANS-based turbulence models on nonlinear wave generation in a two-phase numerical wave tank. *Progress in Computational Fluid Dynamics, na International Journal*, 17(3), 141-158.
https://doi.org/10.1504/PCFD.2017.084350

Faltinsen, O. M. (2015). Hydrodynamics of marine and offshore structures. *Journal of Hydrodynamics*, Ser. B, 26(6), 835-847.
https://doi.org/10.1016/S1001-6058(14)60092-5

Higuera, P. (2016). OLAFOAM Reference Manual.

Jasak, H. (2009). OpenFOAM: open source CFD in research and industry. *International Journal of Naval Architecture and Ocean Engineering*, 1(2), 89-94.
https://doi.org/10.2478/IJNAOE-2013-0011

Kajishima, T., & Taira, K. (2016). *Computational fluid dynamics: incompressible turbulent flows*. Springer.

Könözsy, L. (2019). The k-ω Shear-Stress Transport (SST) Turbulence Model. In *A New Hypothesis on the Anisotropic Reynolds Stress Tensor for Turbulent Flows: Volume I: Theoretical Background and Development of an Anisotropic Hybrid k-omega Shear-Stress Transport/Stochastic Turbulence Model* (pp. 57-66). Cham: Springer International Publishing.
https://link.springer.com/chapter/10.1007/978-3-030-13543-0_3

Kumar, N. K., Savitha, R., & Al Mamun, A. (2018). Ocean wave characteristics prediction and its load estimation on marine structures: A transfer learning approach. *Marine Structures*, 61, 202-219.
https://doi.org/10.1016/j.marstruc.2018.05.007

Lee, D., Park, H., Shin, S., & Cox, D. T. (2021). Experimental and numerical study on the wave, surge, and structure interactions on a coastal residential building. *Journal of Coastal*

Research, 114(SI), 156-160.
https://doi.org/10.2112/JCR-SI114-032.1

Li, J., Zhang, H., Liu, S., Fan, Y., & Zang, J. (2022). Experimental investigations of secondary load cycle formation in wave force on a circular cylinder under steep regular waves. *Ocean Engineering*, 253, 111265.
https://doi.org/10.1016/j.oceaneng.2022.111265

Mo, W., Irschik, K., Oumeraci, H., & Liu, P. L. F. (2007). A 3D numerical model for computing non-breaking wave forces on slender piles. *Journal of Engineering Mathematics*, 58, 19-30.
https://link.springer.com/article/10.1007/s10665-006-9094-6

Mohapatra, S. C., & Soares, C. G. (2019). Interaction of ocean waves with floating and submerged horizontal flexible structures in three-dimensions. *Applied Ocean Research*, 83, 136-154.
https://doi.org/10.1016/j.apor.2018.10.009

Qiu, W., Wang, Z., Jiang, M., & Lin, L. (2022). Prediction approach for wave forces on large-scale offshore structures under linear wave action. *Ocean Engineering*, 257, 111694.
https://doi.org/10.1016/j.oceaneng.2022.111694